Cosine Error Elimination Method for One-Dimensional Convex and Concave Surface Profile Measurements

Xiangyu Guo
J. Mike Walker '66 Department of Mechanical Engineering,
Texas A&M University,
202 Spencer Street,
College Station, TX 77843
e-mail: xiangyug33@tamu.edu

Jaemin Han
J. Mike Walker '66 Department of Mechanical Engineering,
Texas A&M University,
202 Spencer Street,
College Station, TX 77843
e-mail: jaemini2017@tamu.edu

ChaBum Lee[1]
J. Mike Walker '66 Department of Mechanical Engineering,
Texas A&M University,
202 Spencer Street,
College Station, TX 77843
e-mail: cblee@tamu.edu

This paper presents a novel method to eliminate cosine error in precision concave and convex surface measurement by integrating a displacement probe in a precision spindle. Cosine error in surface profile measurement comes from an angular misalignment between the measurement axis and the axis of motion and negatively affects the measurement accuracy, especially in optical surface measurements. A corrective multiplier can solve this problem for spherical surface measurement, but cosine error cannot be eliminated in the case of complex optical surface measurement because current tools do not measure such surfaces along the direction normal to the measurement plane. Because the displacement probe is placed on the spindle axis, the spindle error motion will affect the shape precision and surface roughness measurement of optical components such as mirrors and lenses, and the displacement probe will measure a combination of the spindle error motion and the geometry of optical surfaces. Here, the one-dimensional concave, convex, and hollow measurement targets were used, and cosine error was fundamentally eliminated by aligning the probe on the spindle always normal to the measured surface, and compensation was made for the aerostatic bearing spindle rotational error obtained by the reversal method. The results show that this proposed measurement method cannot only eliminate cosine error but also scan the large area quickly and conveniently. In addition, measurement uncertainty and further consideration for future work were discussed.
[DOI: 10.1115/1.4046078]

Keywords: cosine error, surface metrology, reversal method, spindle error compensation, inspection and quality control, metrology

1 Introduction

In recent decades, high technology developments in computer numerical control (CNC), diamond turning, magnetorheological finishing, ion polishing, and elastic emission machining have removed many difficulties involved in the manufacture of high-accuracy conventional optics [1–6]. Though ultra-precision machining can produce complex-shaped or high-aspect optical parts with high accuracy, profile errors may be caused by many factors, such as environmental factors, machine structural errors, vibration, and tool wear. Any optical surface slope error or surface figure error departure from the theoretical surface will be produced by beam deviations according to Snell's law (law of refraction) for transmission optics or according to the law of mirror reflection. The deviated beam will blur the image quality, enlarge the focus point, degrade the accuracy of the wavefront, and harm the performance of the optical system [7–12]. Therefore, the metrology and compensation are indispensable and fundamental techniques for avoiding such errors and obtaining better performance of the optical systems.

Up-to-date, optical or tactile systems for measuring optical surfaces are the most advanced methods in surface metrology. The results contain systematic errors due to the machine's error motions. In this case, the systematic errors of the machine may be hidden, but cosine error involved in measuring spherical, aspherical, or freeform optical surfaces may be inevitable. Cosine error (ε_C) in surface profile measurement comes from an angular misalignment (θ) between the measurement axis and the axis of motion and negatively affects the measurement accuracy. The schematic diagram is shown in Fig. 1, where d is the actual displacement and d' is the measured displacement

$$\varepsilon_C = d - d', \text{ where } d' = d\cos\theta \tag{1}$$

$$\varepsilon_C = d(1 - \cos\theta) \tag{2}$$

The cosine error increased faster with larger angular misalignment. Figure 2 presents the increasing tendency in cosine error, where we set the actual displacement d as 0.5 mm.

A corrective multiplier can solve this problem for spherical surface measurement, but cosine error cannot be eliminated in the case of aspherical or freeform surface (e.g., Fresnel lenses, gratings, or high-order polynomial surfaces) measurement because current tools do not measure such surfaces along the direction normal to the measurement plane. Measurement of $\lambda/20$ (surface roughness relative to the typical wavelength of operation for an optical part) surfaces is no longer a black art practiced by a master metrologist,

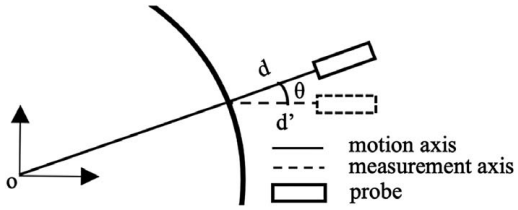

Fig. 1 Schematic diagram of the cosine error effect

[1]Corresponding author.
Manuscript received October 10, 2019; final manuscript received January 14, 2020; published online January 21, 2020. Assoc. Editor: Laine Mears.

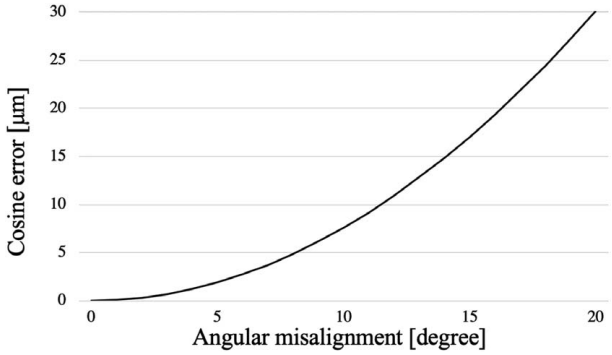

Fig. 2 Cosine error versus angular misalignment distribution

and major tasks for precision metrology of routine or research surfaces have been recently focused on measuring surface roughness with a height resolution of less than 1 Å, with $\lambda/1000$ repeatability [13]. Such high accuracy, however, is limited mainly due to cosine error. Since cosine error leads to critical measurement error in precision metrology of optics manufacturing requiring the highest accuracy, it is urgent that a new rigorous sensing methodology for cosine error-free precision dimensional metrology of optical surfaces be investigated. However, there are few methods to measure the machined optic surfaces with no cosine error.

For a long time, a tactile coordinate measuring machine (CMM) was the first choice for geometric dimensioning and tolerance measurement due to its universality and high accuracy [14]. Currently, no other measuring equipment can be so widely applied in the field of geometric measurement. As versatile as the CMM is, there are still certain workpieces with freeform surfaces, aspheric lenses, that present significant measurement challenges. Although CMMs have been widely used in the manufacture of aspheric lens for quality control, there are shortcomings worth examining. Cai et al. did a thorough analysis on the probe's diameter error [15]. Some of these shortcomings, like the cosine error, can be compensated if the operator can recognize the errors inherent in tactile measurements and manage them to produce accurate results. For example, the measurement of aspheric lenses is normally performed by evaluating their specific section profiles regarding their profile/positioning deviations. These section profiles have specific heights referring to a certain datum and are generated by an aspheric lens formula. These resulting closed 3D planar curves are the section profiles, which are to be inspected. Although these curves are planar, they cannot be treated as 2D curves because the normal direction of each point is always changing in 3D. Due to this feature, the tactile method suffers from cosine error (radius compensation error), and the cosine error cannot be ultimately eliminated.

Moreover, when a ball stylus is used to scan the section profile, the actual contact point with the surface is not the expected one (Fig. 3). The measuring software records the stylus center point coordinates and does a radius compensation afterward to get the actual point coordinates. In this case, the probe is already triggered before the stylus touches the expected point. Therefore, the compensated coordinates will have the cosine error ε_C

$$\varepsilon_C = L - R\cos\ \alpha \tag{3}$$

where L is the distance between the stylus center point coordinate and the expected touching point, R is the radius of curvature of the probe, and α is the angle between the actual touching point and the expected touching point. From Eq. (3), it is very difficult to compensate for cosine error in the case of the freeform surfaces because the physical touching angle α significantly changes. Also, areas smaller than the probe dimension cannot be measured due to physical contact limits. To make things worse, when using a CMM with an analog probe, the normal method of measuring the

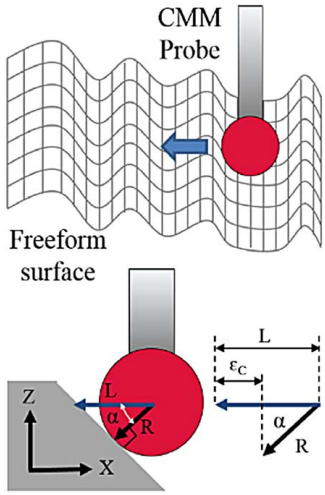

Fig. 3 Cosine error in CMM

location of a point on a surface is to move the CMM so that the probe is deflected by contact with the surface. Also, the roundness of the probe negatively affects the measurement results. As a result, the CMM approach is limited to achieve the desired accuracy due to cosine error, probe deflection, and roundness of the probe. Thus, it is highly desirable that non-contact measuring methods with no cosine error be investigated to determine the optical surface metrology.

Commercially available non-contact surface metrology tools are atomic force microscopy (AFM), white-light interferometry, confocal microscopy, autofocusing microscopy, and phase-shifted microscopy [6]. Such measuring systems are measuring range- or area-limited, and sometimes stitching process is required to measure the whole target surface. Fizeau and Twyman-Green's interferometry, scanning multi-wavelength interferometry like the Luphoscan [16] are common for the whole surface profiles measurements, but such systems require various standard lenses toward different target surfaces, the technical details toward minimizing or eliminating cosine error have not been reported although those systems have been successfully applied and demonstrated to surface measurement with a high accuracy.

Many previous studies have introduced the cosine error compensation methods corresponded to the above techniques, but there is few research to completely eliminate cosine error during the measurements. Gao proposed large-area, micro-structured surface measuring systems based on AFM that compensated for AFM probe directional error with the capacitive sensor and linear encoder [6], and Kang et al. introduced a fiber optics-based Fizeau interferometry and confocal microscopy for surface topography measurement [17]. El-Zaiat et al. measured the radius of curvature of concave and convex mirrors using Twyman-Green's interferometry that does not require the conventional focusing lens in a moving arm [18]. Ennos and Virdee measured a quasi-conical mirror surface profile by scanning the surface with a laser beam and analyzing the variation in reflected beam angle by autocollimation [19]. Rosete-Aguilar and Diaz-Uribe presented a method for testing the profiles of spherical surfaces by measuring the transversal deflection of a reflected laser beam with the optical surface rotations around the axis, located in the center of the surface curvature [20]. Lee et al. introduced the surface straightness profile measurement method for cylindrical targets by using a rotating reversal method from the outputs of two capacitive sensors (CS) [21]. Hou et al. proposed a single-step spatial rotation error technique to separate errors of the surface profile and spindle spatial rotational error by using discrete Fourier transform and harmonic analysis [22]. Zhang et al. applied phase measuring method and error compensation in 3D profile measurement [23].

This study introduces a novel methodology for the machined optical surface metrology that integrates a displacement probe in a precision spindle. To eliminate cosine error, the displacement probe is always placed normal to the measurement target surface by rotating the probe. Spindle rotational error measured by a reversal method [24–27] was compensated for in the surface profile measurement. The 1D optical concave and convex mirror surfaces and bearing bore and outer surfaces as well as the thickness of hollow structure are measured by the proposed method, and the uncertainty sources associated with the proposed measurement method as well as the further work are discussed.

2 Measurement Method

The proposed measurement system illustrated in Fig. 4 consists of an aerostatic bearing spindle, which can achieve higher precision with more controllable spindle error $S(\theta)$, two cylindrical probe-type CS, a sensor holder, and an artifact attached on the spindle shaft. The resolution for the CS is 10 nm, effective sensing area is ϕ5 mm, and the near gap between the CS and the measured target range is 500 μm.

2.1 Reversal Method. Because the rotating accuracy of a spindle directly affects the CS 2 output, the spindle error $S(\theta)$ was separated from the part (artifact) error $R(\theta)$ by a reversal method proposed by Donaldson [24] and Bryan et al. [27] as shown in Figs. 4(*a*) and 4(*b*). First, the artifact is positioned at an arbitrary angular position on the spindle, and a roundness trace is acquired from CS 1. Then, the CS 1 and the artifact are rotated by 180 deg. A new roundness trace is then acquired. Figures 4(*a*) and 4(*b*) show the two reversal positions. In position 1 (Fig. 4(*a*)), the CS 1 reads a measured signal $m_1(\theta)$ given by

$$m_1(\theta) = R(\theta) + S(\theta) \tag{4}$$

In position 2 (Fig. 4(*b*)), the CS 1 reads a measured signal $m_2(\theta)$ given by

$$m_2(\theta) = R(\theta) - S(\theta) \tag{5}$$

Then, the part and spindle errors can easily be obtained as

$$R(\theta) = (m_1(\theta) + m_2(\theta))/2 \tag{6a}$$

$$S(\theta) = (m_1(\theta) - m_2(\theta))/2 \tag{6b}$$

2.2 Surface Profile Measurement. After separating spindle error from the part error, the measurement target (mirror surface with a radius of curvature, R_0) is placed with the offset distance from the spindle rotational axis that is the same as a radius of curvature of the measurement target, and its surface profile can be obtained by rotating the spindle. This measurement allows for the measurement probe to be always placed toward the measurement target surface at a right angle. However, because this surface profile information includes spindle error, the corrected surface profile can be expressed as

$$G(\theta) = R_0 + \Delta D(\theta) - S(\theta), \text{ where } \Delta D(\theta) = D(\theta) - D_0 \tag{7}$$

where R_0 is the radius of curvature of the measurement target and D_0 is the initial offset distance of CS 2 at the beginning of the measurement. The surface profile $\Delta G(\theta)$ that subtracts R_0 from $G(\theta)$ can be calculated as

$$\Delta G(\theta) = G(\theta) - R_0 \tag{8}$$

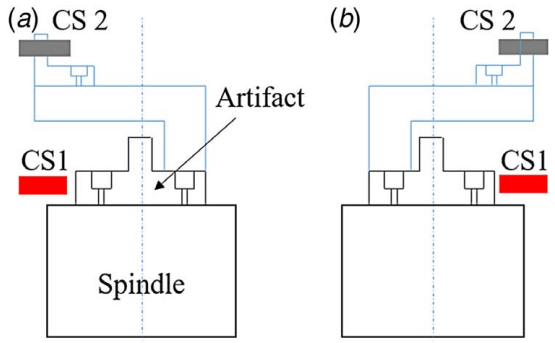

Fig. 4 The proposed surface profile measurement method: part error $R(\theta)$, spindle error $S(\theta)$, sensor output $D(\theta)$, and surface profile $G(\theta)$

3 Experiment

3.1 Spindle Error Separation. The experiment setup is shown in Fig. 5. The measurement was performed in a vibration-controlled lab environment. An aerostatic bearing spindle (Dover Instrument) and two identical capacitive sensors (10 nm resolution, effective sensing area ϕ 5 mm) are employed for the experiment. To eliminate the spindle dynamic effects and brushless direct current (DC) motor effects, the measurement data was discretely collected from the equally spaced points of the target surface and was averaged. Surface profiles of the concave (R_0 95 mm) and convex (R_0 100 mm) cylindrical lenses (United Scientific Supplies Inc.) and precision thrust bearing (Koyo 51211, bore R_0 27.5 mm, outer R_0 45 mm) were measured by the proposed measurement system. Although their surface profiles include form error, waviness error, and roughness along the radial direction, the manufacturers provide only the representative values such as radius and tolerance of their surfaces. Thus, their surface profile information is uncertain.

Spindle error was separated by the reversal method as shown in Fig. 6. The spindle motion was measured every 10 deg interval twice. From Eq. (7), the standard deviation of spindle error $S(\theta)$ was 0.081 μm, and its peak-to-valley (PV) value was 0.298 μm. Also, the standard deviation of part error $R(\theta)$ was 0.217 μm, and its PV value was 0.786 μm.

3.2 Cylindrical Concave and Convex Lens Profile Measurement. As depicted in Fig. 7, after separating the spindle error from the part error, the displacement probe scans the cylindrical mirror, and then, the surface profile $\Delta G(\theta)$ that subtracts R_0 from $G(\theta)$ can be calculated from Eq. (8). The aluminum film was adhered to the acrylic cylindrical concave and convex lenses to make it conductive for capacitance measurement between the probe and target surfaces. Concave and convex target surfaces were placed 95 mm and 100 mm away from the center of the spindle rotational axis for each measurement, respectively. While rotating the spindle axis that can make the measurement probe always be placed normal to the target surface, each target surface was measured three times with an equal interval of 5 mm over 87 mm. From the results shown in Fig. 8, the PV value for the

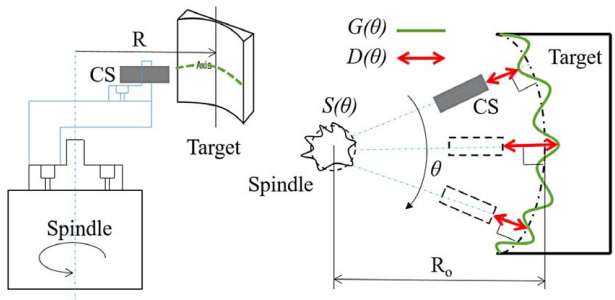

Fig. 5 The proposed surface profile measurement method

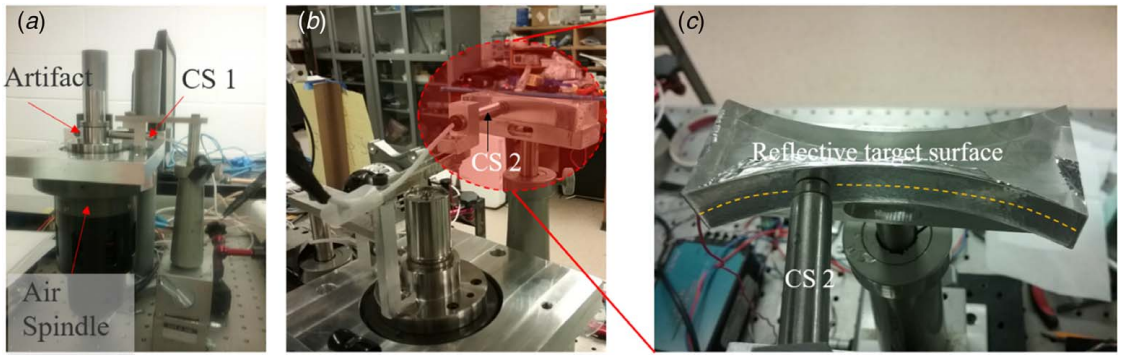

Fig. 6 Experimental setup: (*a*) spindle error separation setup, (*b*) full setup for surface profile measurement, and (*c*) detailed image

concave surface profile was approximately 27 μm, and the measurement standard deviation (averaged from three measurement results) was calculated at 0.24 μm (Fig. 8(*b*)). Because the measurement method depicted in Fig. 5 is for a concave surface, a modified measurement setup for convex measurement is proposed as shown in Fig. 9. As a result, the PV value for a convex surface profile was approximately 210 μm, and the measurement standard deviation (averaged from three measurement results) was calculated at 3.40 μm (Fig. 10).

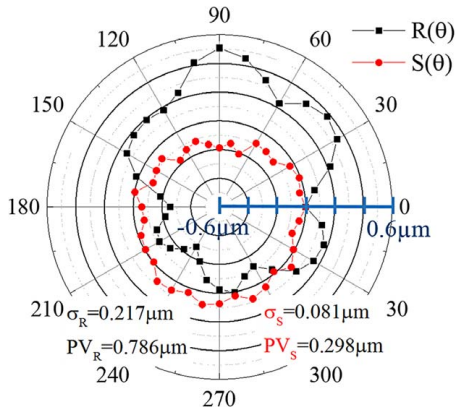

Fig. 7 Result of spindle error separation

In the proposed measurement method, placing the target surface at the correct position (the same as the radius of curvature of each target) from the spindle rotation axis is critical to the surface profile measurement. Because there may exist spindle rotation axis-to-target surface positioning error, the effects of positioning error on surface profile measurement were investigated by measuring the surface profile at various positions along the *Z*-axis as shown in Fig. 11.

The radial offset distance between spindle rotation axis and target surface varies from -100 μm to $+100$ μm (at a given distance R_0), and the manual linear stage with the micrometer was used to move the target surface forward and backward. This offset distance from -100 μm to $+100$ μm was selected because such positioning accuracy of the target surface can be easily achieved, even manually, in measurement alignment processes. Similar to the previous measurements in Figs. 8 and 10, each target surface was measured at an equal interval of 5 mm over 87 mm. Also, the measurement data were discretely collected from the equally spaced points of the target surface and were averaged to eliminate the spindle dynamic effects and brushless DC motor effects. From the result of Fig. 12, at a given offset distance (± 100 μm), the measured surface profiles showed trends over the offset distances for both concave and convex surfaces. These results indicate that the proposed measurement method is effective for measuring both the concave and convex surfaces and is not significantly sensitive to the radial offset distance between the spindle rotation axis and the measurement target surface.

3.3 Bearing Surface Profile Measurement. The proposed measurement method was applied to the bearing surface profile

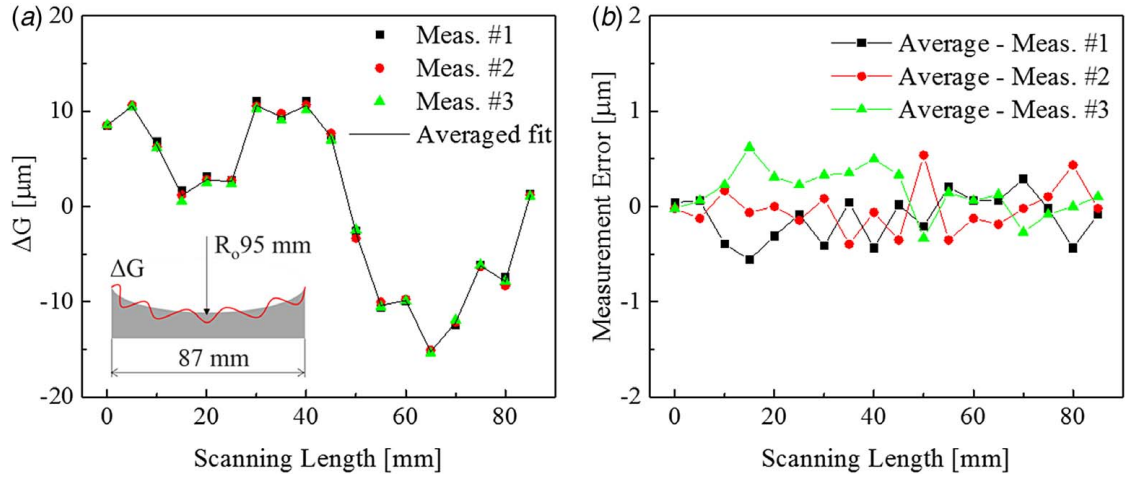

Fig. 8 Surface profile measurement results of concave lens R_0 95 mm: (*a*) surface profile and (*b*) measurement deviation

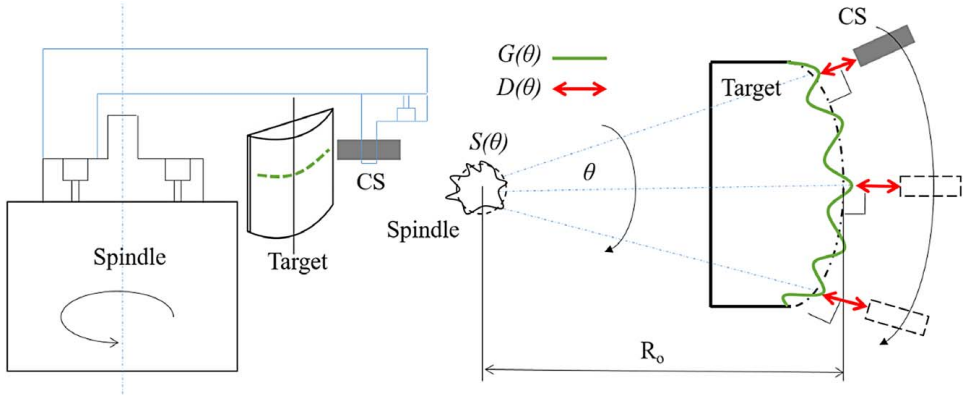

Fig. 9 A modified setup for convex surface profile measurement

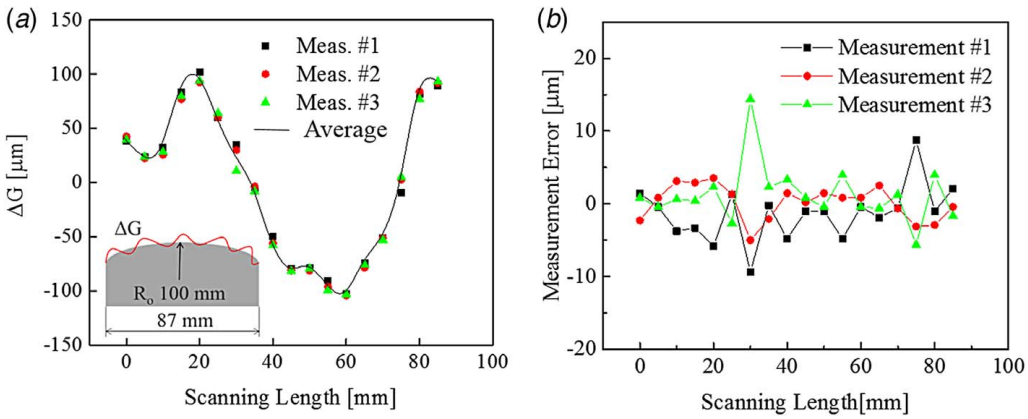

Fig. 10 Surface profile measurement results of convex lens R_0 100 mm: (*a*) surface profile and (*b*) measurement deviation

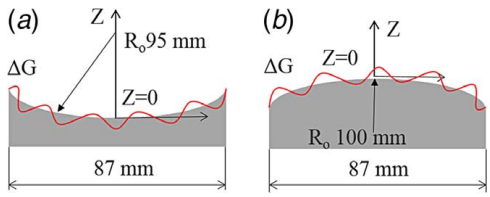

Fig. 11 Illustration of lens surface profiles: (*a*) concave and (*b*) convex

measurement. As shown in Fig. 13, bore and outer radii of bearing (Koyo, 51211) are 27.5 mm ± 15 μm and 45.0 mm ± 5 μm, separately. Here, for bore-surface profile measurement, the measurement method for concave surfaces (Fig. 5) was used, and the measurement method for convex surfaces was used for outer-surface profile measurement. Similar to the lens surface profile measurement, the surface profiles $\Delta G(\theta)$ for the bore and outer surface were obtained from Eq. (7). The bearing bore and outer surfaces were measured at every 5 deg interval from −70 to + 70 deg. The PV were approximately 23 μm and 4 μm for bore and outer surfaces, and the RMS value were approximately 7 μm and 1 μm for bore and outer surfaces, respectively.

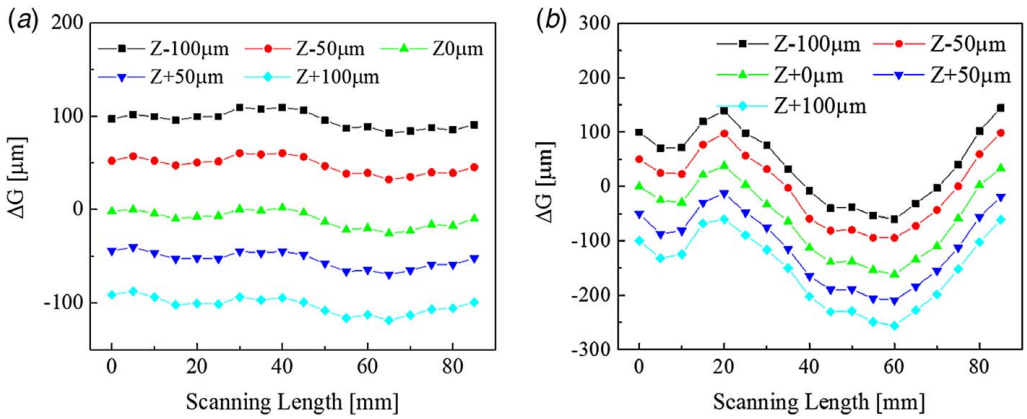

Fig. 12 Measurement target surface positioning effects on surface profiles: (*a*) concave and (*b*) convex

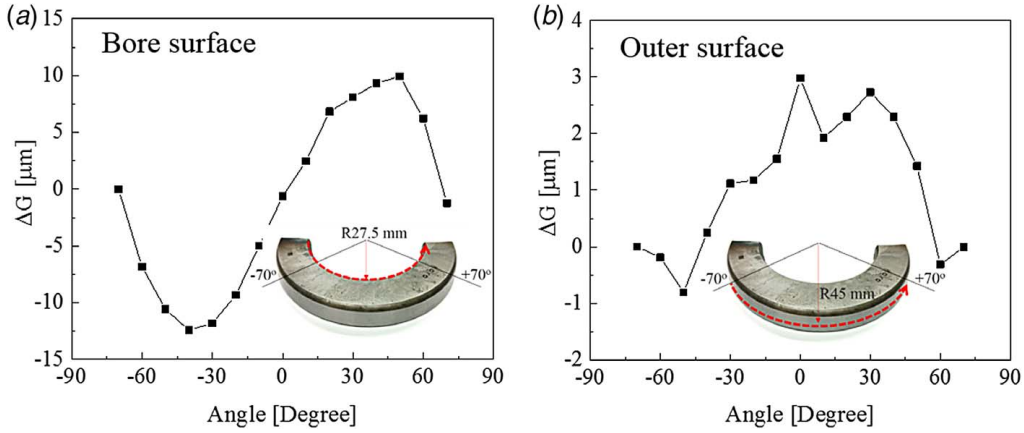

Fig. 13 Measurement results of bearing surface profiles: (*a*) bore surface and (*b*) outer surface

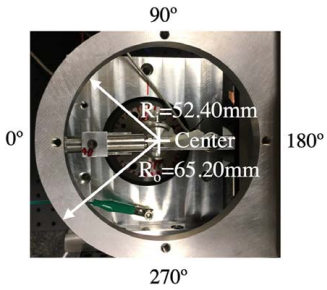

Fig. 14 Measurement target information

3.4 360 Degrees Surface Profile Measurement. The proposed method was applied to the 360 deg surface profile measurement and the thickness (between inter surface and outer surface) measurement on a hollow structure. The measurement sample was manufactured by a general-purpose milling machine. As shown in Fig. 14, the radii of the concave (inner surface) and convex (outer surface) profiles are 52.40 mm (R_i) and 65.20 mm (R_o), respectively. The difference in the radius becomes the thickness of the measurement target. Each surface profile was measured three times by 10 deg interval, and then, the measurement data were averaged.

The probe was aligned with the spindle rotational axis, and the measurement range is 360 deg for the concave target and 100 deg for the convex target. Figure 15(*a*) presents the averaged result of the deviation of the surface profiles (μm), the PV value for the deviation was approximately 237 μm. Figure 15(*b*) shows the measured radii (mm). The maximum deviation δ of three measurements was at the 300 deg, which was 3 μm, and the measurement standard deviation $\sigma_{meas.}$ was 0.5 μm.

Figure 16 presents the measured results of the deviation of the surface profile. This hollow structure is manufactured by the general purposed CNC machine tool, the surface PV deviation is 1.13 mm, which is the manufactured error. The maximum deviation δ of three measurements was at 30 deg, which was 3 μm, and the measurement standard deviation $\sigma_{meas.}$ was 0.77 μm.

3.5 Thickness Measurement. The thickness D can be calculated by

$$D = (R_o + \Delta G_o) - (R_i + \Delta G_i) \tag{9}$$

where R_o and R_i are the nominal outer and inner surface radii, ΔG_o and ΔG_i are averaged outer and inner surface profile corresponded to each point. Figure 17 shows the thickness in the range from 310 to 50 deg, and the maximum deviation from the thickness distribution was 1.101 mm.

From above, the proposed technique is able to finish the surface profiles measurement, 360 deg surface profiles measurement as well as the thickness measurement without moving the target surfaces.

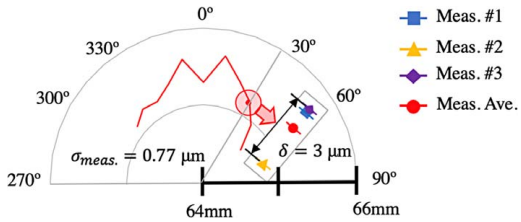

Fig. 16 Surface measurement results

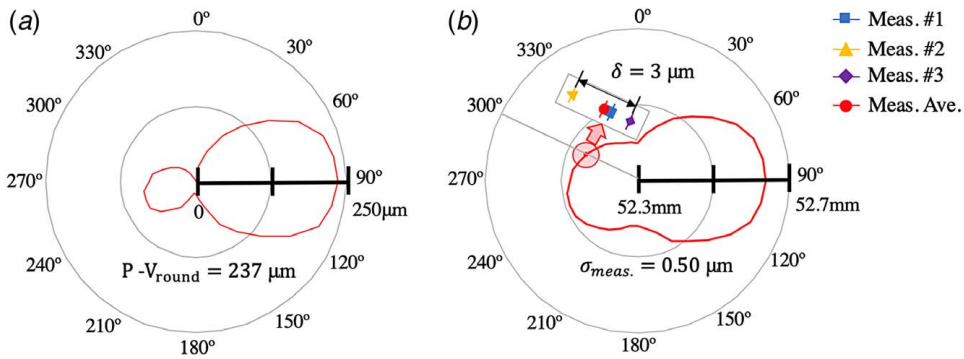

Fig. 15 Concave surface averaged measured 360 deg surface profiles results (*a*) and the radii R results (*b*)

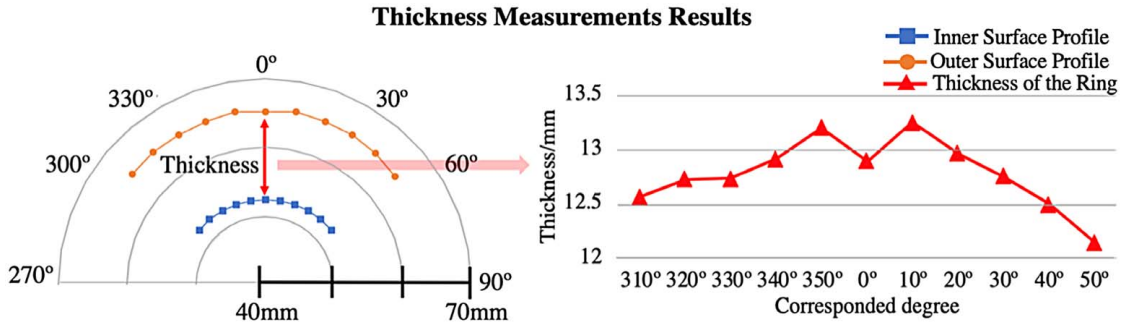

Fig. 17 Thickness measurement results

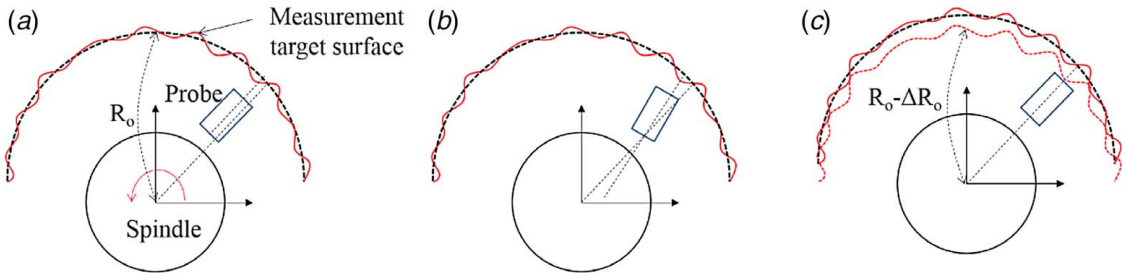

Fig. 18 Measurement uncertainty sources (alignment errors): (*a*) probe offset error, (*b*) probe angular alignment error, and (c) target positioning error

4 Uncertainty Evaluation

The measurement uncertainty can be estimated by the measurement limits at a given confidence level because the error source is typically unknown and unknowable. Here, four main uncertainty sources were considered: instrumentation, installation (Figs. 18 and 19), environment, and rotational motion. Each uncertainty sources are discussed. Measurement uncertainty of the proposed system depending on the probe type was analyzed 1.04 μm in Table 1.

4.1 Instrumentation Error. In this experiment, the CS and 16-bit data acquisition units (National Instruments USB 6351) were used. The sensitivity and the noise level (resolution) of the CS are 11.99 mV/μm and 0.05 μm, and the quantization error (a half of digital resolution) of the data acquisition unit can be estimated at 0.006 μm.

4.2 Installation Error. For the installation error, as a part of the measurement uncertainty estimation of the proposed system, the surface profile error could result from three alignment errors as illustrated in Fig. 18, which are the probe offset error (Fig. 18(*a*)), probe angular alignment error (Fig. 18(*b*)), and the target positioning effect (Fig. 18(*c*)), where R_o is the nominal radius. In this study, the probe with an effective sensing area of ϕ 4 mm was used.

To investigate the effect from the alignment errors, the probe offset varied range from the original position was $\pm$100 μm, the

Table 1 Uncertainty budget of the surface profile measurement

Uncertainty source	Details	Calculation	Uncertainty (μm)
Instrumentation error (type B uncertainty)	Capacitive sensor	u_{I1} = noise level (RMS value)	0.05
	Data acquisition quantization error	$u_{I2} = \frac{\text{output voltage range}}{2 \times 2^{16} \times \text{sensitivity}} = \frac{10\text{ V}}{2 \times 2^{16} \times 11.99\text{ mV}/\mu\text{m}}$	0.006
Installation error (type A uncertainty)	Probe offset error	Fig. 19(*a*)	0.47
	Probe angular error	Fig. 19(*b*)	0.78
	Target positioning error	Fig. 19(*c*)	0.48
Environmental error (type B uncertainty)	Thermal drift (sensor)	u_{E1} = 80 ppm/°C[2]	0.008
	Thermal drift (spindle)	u_{E2} = 90 ppm/°C [28]	0.009
	Air pressure	Air pressure level was well regulated	Not considered
	Ground vibration	Experiment was performed in a vibration-isolated granite table	Not considered
Rotational error (type—A uncertainty)	Spindle error	Fig. 7 (should add along with the Abbe error)	0.081
Total uncertainty	95% confidence level (k = 2) design stage uncertainty	$\sqrt{0.05^2 + 0.006^2 + 0.47^2 + 0.78^2 + 0.48^2 + 0.008^2 + 0.009^2 + 0.081^2}$	1.04

[2]https://www.capacitec.com/Displacement-Sensing-Systems

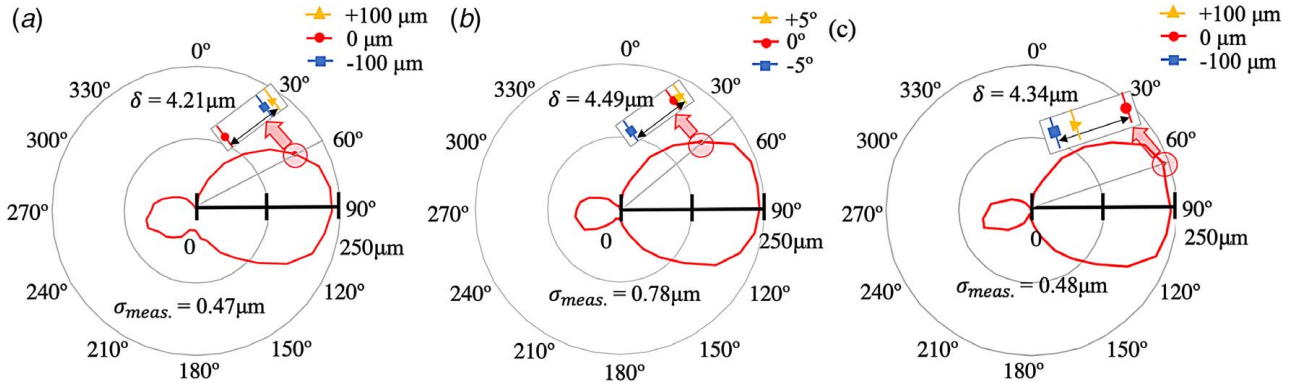

Fig. 19 Installation uncertainty results: (*a*) probe offset, (*b*) probe angular alignment, and (c) target positioning offset

probe angular deviation was ±5 deg, and the target offset was ±100 μm, this will allow the positioning accuracy to easily achieve. Taking the example of the hollow structure's inner surface (concave) profile measurement, the probe was aligned with the spindle rotational axis first, the offset distance was set to be the same as the nominal radius of curvature of the measurement target. For case Figs. 18(*a*) and 18(*c*), adjusting the offset of the target position by using the micrometer in the lateral and vertical directions. For case Fig. 18(*b*), adjusting the tilt of the probe by using the indicator on the target surface. The uncertain test results are shown in Fig. 19, the surface was measured by 10 deg interval.

The measured surface profiles show the same trends over the range of the offset distance and tilted angle, which can be observed from the radii distribution (Fig. 19). Shifting or rotating back the measured offset surface profiles to the aligned position, the maximum deviations δ among each measured point were 4.21, 4.49, and 4.34 μm for case Figs. 19(*a*)–19(*c*), and the measured standard deviations (averaged value of standard deviation from each measured point) among the initial and shifted or rotated back positions were 0.47, 0.78, and 0.48 μm, individually.

4.3 Environmental Error. The lab temperature was stable at 23 °C with 1 °C temperature variation. Compressed air was regulated for the spindle system and a vibration-isolated granite table was applied for the experiment setup. Humidity variation was not considered. The thermal drift affects the sensor and the aerostatic bearing spindle. Those uncertainty values were found from Refs. [28].[3]

4.4 Rotational Error. The measurement rotational error here corresponds with the spindle error in Fig. 7. It was separated by the reversal method, the spindle motion was measured every 10 deg interval twice. The spindle error can be one of measurement uncertainty sources in this measurement method.

5 Comparison With Coordinate Measuring Machine

Table 2 compared the measured surface PV profiles deviation and the thickness results with the CMM (Mitutoyo CRYSTA-APEx C 7106)[4] and the SP25M stylus (4 × 50 mm). The corresponded probing permissible error is $1.7 + 4L/1000$ μm, where L is the selected measuring length (in mm), and the permissible scanning error is 2.3 μm. Based on the specifications, the measurement uncertainty estimated is 2.86 μm, on the other hand, the measurement uncertainty of the proposed measurement system is 1.04 μm.

Both the CMM's uncertainty and inevitable cosine error may result in some discrepancy with the measurement results of the proposed measurement system, although such discrepancy does not seem to be critically large. Although the measurement samples have their own form error, waviness error, and roughness along the radial direction, their surface profile information is uncertain because the manufacturers do not provide the surface information but only radius and tolerance of their surfaces. Thus, the true values of those measurement samples are unknown. Here, the results obtained by the proposed measuring system were compared with those of the CMM. The comparison data in Table 2 indicates that two measuring systems showed good agreement in the micrometer scale, which is the resolution of the CMM used in this study.

Table 2 Surface PV profiles deviation and the thickness measured results comparison

Instrument	Cylindrical concave surface	Cylindrical convex surface	Bearing bore surface	Bearing outer surface	Hollow thickness
CMM	24 μm	235 μm	23 μm	7 μm	12.73 mm
Proposed technique	27 μm	210 μm	23 μm	4 μm	12.75 mm

Because there always exists a discrepancy in all measurement results due to each measuring system's uncertainty, measurement sample setting, and even accuracy error due to outdated calibration, it is too early to draw the conclusion that cosine error elimination could improve measurement uncertainty. However, as seen in Fig. 2, cosine error significantly increases with respect to the angle normal to the measurement target surface and there is cosine error inevitable in CMM, thus, there is evidence that measurement uncertainty is partially associated with cosine error.

6 Further Consideration

This measurement technique can be easily applied to 1D concave and convex target profile measurements. As the commercial offered values for the profiles of the sample are always constant, here we assumed the surface profile is constant. While in practical manufacturing process, the value is varied, in the proposed method, we take this effect into account of the uncertainty analysis. As this installation error is the main contribution of the total uncertainty, to improve the performance of the proposed technique, an extra designed alignment guide for the sensor is required.

Apart from that, the sensing area of the capacitance sensors limits the interval range and the displacement measuring range limits the range of the surface profile variation. Alternatively, a laser displacement sensor with a smaller sensing area (~μm) can be used in the future, and the proposed measurement technique combined with multi-axis precision motion control will allow for freeform surface measurement.

For the next development, the proposed measurement system can be integrated with machine tools for on-machine

[3]See Note 2.

[4]https://www.mitutoyo.com/wp-content/uploads/2013/01/2097_CRYSTA_ApexS.pdf

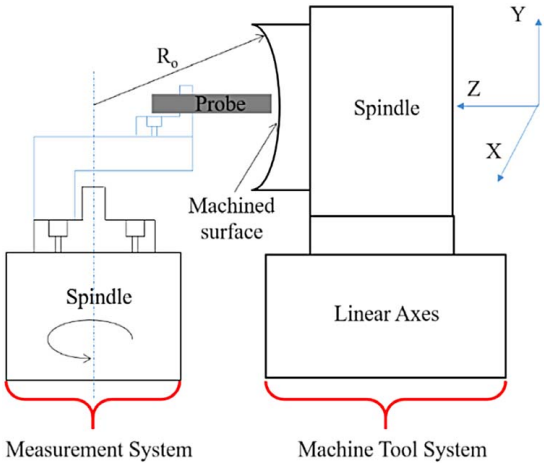

Fig. 20 An on-machine measurement application for freeform surface metrology

measurement (OMM) applications. The integration of metrology in manufacturing processes is becoming increasingly important. OMM can avoid the errors caused by moving and re-positioning the workpiece and can use the machine axes to extend the measuring range and improve the measuring efficiency [2,13]. OMM tools will measure the machined surface following the trajectory given by the same CNC commands. The benefit of OMM preserves the consistency between the machining and measurement coordinate system with the goal of further improving the surface accuracy and corrective machining is carried out based on the on-machine measured data [29].

For example, as illustrated in Fig. 20, if *XZ* axes and the OMM spindle are simultaneously controlled, surfaces, even freeform surfaces, can be measured with no cosine error using the proposed measurement method. This will solve cosine error-related measurement issues because the OMM tools measure the machined surface along the direction normal to the measurement plane. It will be interesting to investigate the OMM systems' performance boundaries in providing the correct CNC codes that reduce measurement error down to nanometer or sub-nanometer levels in surface measurement involved in compensation machining.

7 Conclusion

A novel, fast, large-area, high precision measurement method capable of eliminating cosine error, especially for optical surface metrology, was proposed and validated. The precision manufactured artifacts, concave mirror, convex mirror, and bearing inner and outer surfaces were measured, and the experiment results were compared with those of CMM. Two results showed good agreement within a few micrometers. Spindle rotational error was compensated for the surface profile data by using the reversal method. As a result, it was confirmed that the proposed measurement system can apply for measuring both concave and convex surface profiles and has a potential for thickness profile measurement applications. In addition, the proposed measuring system can scan the large area quickly and conveniently by thoroughly eliminating the cosine error and improving the system performance. With these implements, in the future, the proposed measurement system can be used for freeform surface measurement by integrating this measurement method with precision machine tools for OMM applications. It will not only reduce measurement error but also improve manufacturing performance by simultaneously providing correct CNC codes for compensation machining.

Acknowledgment

The research was supported by the National Science Foundation (Award No: CMMI 1663210) through the Texas A&M University, and the authors would like to thank Dr. Tony L. Schmitz at the University of Tennessee at Knoxville and Dr. Joshua A. Tarbutton at the University of North Carolina at Charlotte for valuable comments.

References

[1] Lasemi, A., Xue, D., and Gu, P., 2010, "Recent Development in CNC Machining of Freeform Surfaces: A State-of-the-Art Review," Comp.-Aided Des., **42**(7), pp. 641–654.
[2] Lin, R.-S., and Koren, Y., 1996, "Efficient Tool-Path Planning for Machining Free-for Surfaces," Trans. ASME, **118**(1), pp. 20–28.
[3] Suresh, K., and Yang, D., 1994, "Constant Scallop-Height Machining of FreeForm Surfaces," ASME J. Eng. Ind., **116**(2), pp. 253–259.
[4] Kim, J., and Lee, S.-K., 2016, "Micro-Patterning Technique Using a Rotating Cutting Tool Controlled by an Electromagnetic Actuator," Int. J. Mach. Tools Manuf., **101**, pp. 52–64.
[5] Kim, J., Zhao, S., Kim, G., and Lee, S.-K., 2013, "Rolling Bearing-Suspended Spindle Run-Out Control Using Repetitive Control and Adaptive Feedforward Cancelation," Int. J. Precis. Eng. Manuf., **14**(12), pp. 2171–2178.
[6] Gao, W., 2010, *Precision Nanometrology: Sensors and Measuring Systems for Nanomanufacturing*, Springer, New York.
[7] Simunovic, G., Svalina, I., Simunovic, K., Saric, T., Havrlisan, S., and Vukelic, D., 2016, "Surface Roughness Assessing Based on Digital Image Features," Adv. Prod. Eng. Manag., **11**(2), pp. 93–104.
[8] Gordon, H. R., and Wang, M., 1992, "Surface Roughness Considerations for Atmospheric Correction of Ocean Color Sensors. I: The Rayleigh-Scattering Component," Appl. Opt., **31**(21), pp. 4247–4260.
[9] Harvey, J. E., Schröder, S., Choi, N., and Duparré, A., 2012, "Total Integrated Scatter From Surfaces With Arbitrary Roughness, Correlation Widths, and Incident Angles," Opt. Eng., **51**(1), p. 013402.
[10] Bennett, H. E., and Porteus, J. O., 1961, "Relation Between Surface Roughness and Specular Reflectance at Normal Incidence," J. Opt. Soc. Am., **51**(2), pp. 123–129.
[11] Davies, H., 1954, "The Reflection of Electromagnetic Waves From a Rough Surface," Proc. IEEE. Pt. III, **101**(7), pp. 209–214.
[12] Bennett, H. E., 1963, "Specular Reflectance of Aluminized Ground Glass and the Height Distribution of Surface Irregularities," J. Opt. Soc. Am., **53**(12), pp. 1389–1394.
[13] Qian, S., and Takacs, P., 2012, "Nano-Accuracy Surface Figure Metrology of Precision Optics," *Modern Metrology Concerns*, L. Cocco, ed., InTech. https://www.intechopen.com/books/modern-metrology-concerns/nanoaccuracy-surface-figure-metrology-of-precision-optics, Accessed January 27, 2020.
[14] BS ISO 230-10:2011, 2011, Test Code for Machine Tools Part 10: Determination of the Measuring Performance of Probing Systems of Numerically Controlled Machine Tools, International Standard.
[15] Cai, Z., Luo, Z., and Liu, H., 2019, "Probe Error Analysis of Articulated Arm Coordinate Measuring Machine," Proceedings of SPIE 11053, Tenth International Symposium on Precision Engineering Measurements and Instrumentation, p. 1105339.
[16] Berger, G., 2016, Non-contact 3D Scanning Approach to Solve Measurement Challenges, World Metrology Day, Singapore.
[17] Kang, J.-H., Lee, C., Joo, J.-Y., and Lee, S.-K., 2011, "Phase-Locked Loop Based on Machine Surface Topography Measurement Using Lensed Fibers," Appl. Opt., **50**(4), pp. 460–467.
[18] El-Zaiat, S. Y., Missotten, L., and Engelen, J., 1991, "Radius of Curvature Measurement by Twyman-Green's Interferometer," Opt. Lasers Eng., **15**(3), pp. 203–208.
[19] Ennos, A. E., and Virdee, M. S., 1982, "High Accuracy Profile Measurement of Quasi-Conical Mirror Surfaces by Laser Autocollimation," Precis. Eng., **4**(1), pp. 5–8.
[20] Rosete-Aguilar, M., and Diaz-Uribe, R., 1993, "Profile Testing of Spherical Surfaces by Laser Deflectometry," Appl. Opt., **32**(25), pp. 4690–4697.
[21] Lee, J. C., Noh, Y. J., Ari, Y., Gao, W., and Park, C. H., 2009, "Precision Measurement of Cylinder Surface Profile on an Ultra-Precision Machine Tool," Meas. Sci. Rev., **9**(2), pp. 49–52.
[22] Hou, M., Qiu, L., Zhao, W., Wang, F., Liu, E., and Ji, L., 2014, "Single-Step Spatial Rotational Error Separation Technique for the Ultraprecision Measurement of Surface Profiles," Appl. Opt., **53**(3), pp. 487–495.
[23] Zhang, Y., Zhang, Z., Li, Y., Zhou, W., He, Y., and Li, W., 2019, "Phase Measuring Method and Error Compensation in 3D Profile Measurement," Proceedings of SPIE 11053, Tenth International Symposium on Precision Engineering Measurements and Instrumentation.
[24] Donaldson, R. R., 1972, "A Simple Method for Separating Spindle Error From Test Ball Roundness Error," Ann. CIRP, **21**(1), pp. 125–126.
[25] Marsh, E. R., 2010, *Precision Spindle Metrology*, DEStech Publication Inc., Lancaster, USA.
[26] Muralikrishnan, B., and Raja, J., 2009, *Computational Surface and Roundness Metrology*, Springer, New York.
[27] Bryan, J., Clouser, R., and Holland, E., 1967, "Spindle Accuracy," Amer Mechanist, pp. 149–164.
[28] Tan, B., Mao, X., Liu, H., Li, B., He, S., Peng, F., and Yin, L., 2014," Int. J. Mach. Tools Manuf., **82–83**, pp. 11–20.
[29] Li, D., Jiang, X., Tong, Z., and Blunt, L., 2019, "Development and Application of Interferometric On-Machine Surface Measurement for Ultraprecision Turning Process," ASME J. Manuf. Sci. Eng., **141**(1), p. 014502.